Electronic structure of epitaxial graphene grown on stepped Pt(997)

M. Pisarra,[1] D. Pacilé,[1,2,*] P. Moras,[2] P. M. Sheverdyaeva,[2] A. Sindona,[1,3] M. Papagno,[1,2] and C. Carbone[2]

[1]*Dipartimento di Fisica, Università della Calabria, 87036 Arcavacata di Rende (CS), Italy*

[2]*Istituto di Struttura della Materia, Consiglio Nazionale delle Ricerche, Trieste, Italy*

[3]*INFN - Gruppo collegato di Cosenza, 87036 Arcavacata di Rende (CS), Italy*

(Received 10 December 2013; revised manuscript received 14 March 2014; published 23 May 2014)

Angle-resolved photoemission spectroscopy, low-energy electron diffraction, and density functional theory calculations were employed to investigate the electronic and structural properties of a graphene layer grown on the regularly stepped Pt(997) surface. The measurements show the predominance of a (2×2) multidomain superstructure of graphene, lying flat on the Pt terraces and covering the step edges in a carpetlike mode. The linearly dispersing π band of graphene appears to be weakly affected by the substrate at the K point, while an appreciable hybridization is found at the Γ point. Replicas of the Dirac cone are seen perpendicularly to the steps, with double real-space periodicity compared to the Pt terrace width.

DOI: 10.1103/PhysRevB.89.195438 PACS number(s): 73.22.Pr, 71.15.−m, 79.60.Ht

I. INTRODUCTION

The synthesis of graphene (G) on transition metal surfaces is widely studied in order to obtain well-defined large-area samples, as well as to understand on a basic level the complex G-metal interaction [1–3]. High quality epitaxial G films have been obtained on several transition metal surfaces, ranging from strongly interacting $3d$ metals (such as Ni, Co, and Fe [4,5]) to weakly interacting $5d$ ones (e.g., Ir and Pt [6–9]). Among all metals, the growth of G on Pt(111) has received considerable interest as the Pt substrate marginally affects the characteristic physical properties of graphene. Several studies on the structural and electronic properties of G/Pt(111) have been carried out so far [10–16], which report different moiré superstructures and rotated graphene domains, with nearly unaffected π band dispersion [11,17], and lying at relatively large distances from the substrate (above 3 Å).

In this paper, we present an analysis of the electronic structure of a graphene layer grown on the stepped Pt(997) surface by angle-resolved photoemission (ARPES) and density functional theory (DFT). Vicinal faces of single crystals allow to introduce confinement effects on a large scale, by means of equally oriented steps, and to study possible repercussions on the electron dispersion along the two directions of interest, parallel and perpendicular to the step edges. Indeed, recent ARPES experiments have shown that, due to the step periodicity, surface states can either develop perpendicularly to the steps, showing a repeated band structure with the periodicity of the step [18,19], or behave as nondispersive quantum-well states [20]; these states exhibit peculiar symmetry properties with respect to either the normal to the single terrace or to the macrosurface normal [21].

Concerning the growth of graphene, a vicinal surface might allow the synthesis of graphene nanoribbons, which have attracted considerable interest due to their semiconducting behavior derived from lateral electron confinement [22,23]. Nanoribbon growth has been recently achieved on Au(788) by using dibromo precursor monomers [24], which are sublimated on the clean surface and thermally activated until they form linear chains on the gold terraces. On the other hand, chemical vapor deposition (CVD) of hydrocarbons has been employed on the stepped Ni(771) surface [25], and single domains of strongly interacting (1×1) graphene stripes on the Ni terraces have been found. In the present study, we show that the CVD procedure on Pt(997) yields a multidomains graphene growth with a prevalent (2×2) superstructure, extending across the step edges and thus keeping the two-dimensional character of the graphene layer. Indeed, the dispersion of the π band suggests that nanoribbons are not formed and allows to extract the effect of the periodic steps; along the direction perpendicular to the steps, we identify repeated π bands with double real-space periodicity with respect to the terrace width. In order to explain this behavior, we provide a qualitative structural model. Further, we give a theoretical description of the G/Pt interaction mechanism for the prevalent (2×2) superstructure.

II. METHODS

The experiments were performed at the VUV beamline of the Elettra synchrotron radiation laboratory (Trieste, Italy). The Pt(997) crystal was cleaned using alternated cycles of Ar ion sputtering and annealing at 900 K, followed by slow cooling (at an average rate of 0.5 K per second) and exposures to oxygen at 750 K. This procedure generates contaminant-free surfaces, with large regularly stepped domains [Fig. 1(b)]. The graphene sheet was grown by cracking of ethylene at 700 K. Different exposures of the surface to a dose ranging from 10 to 1000 Langmuir (L) results in similar electronic and structural properties. Therefore, in analogy with graphene on Pt(111), the growth process under our experimental conditions of temperature and dose appears to be self-limited in correspondence with the formation of the first graphene layer. The angle-resolved photoemission data were collected at room temperature with an R4000 electron energy analyzer at photon energies of about 125 and 160 eV, where the contrast between the C and Pt related bands was optimal. Total energy and angular resolutions were 100 meV and 0.3° (0.03 $Å^{-1}$), respectively.

On the theoretical side, the band structure of G/Pt(111) was calculated, with reference to that of freestanding graphene, by a DFT approach based on the local density approximation

*daniela.pacile@fis.unical.it

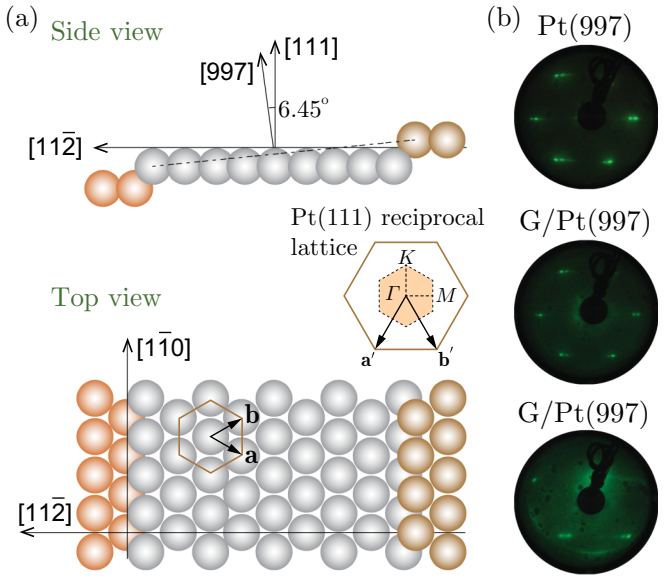

FIG. 1. (Color online) (a) Schematic of the Pt(997) surface in real space (side and top view) and reciprocal space. Pt(111) unit vectors are designed by **a** and **b** in real space, and **a′** and **b′** in reciprocal one. The average step separation is 20.1 Å [34,35]. (b) LEED images of Pt(997) (top), G/Pt(997) (center, and bottom in off normal geometry), at 60 eV of electron beam energy.

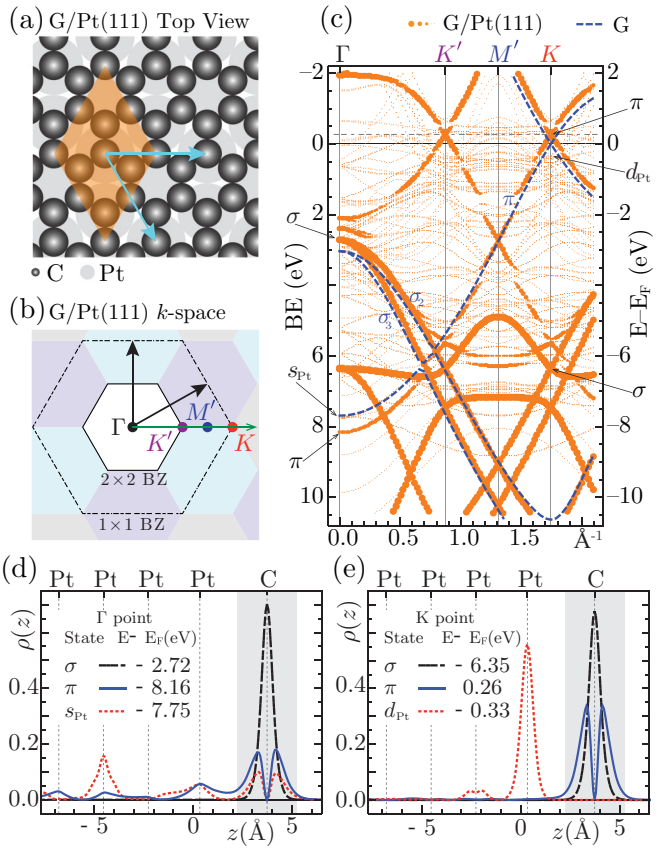

FIG. 2. (Color online) Structural and electronic properties of the (2 × 2)G/Pt(111) interface as computed with the DFT approach outlined in the main text. (a) Top view of the surface geometry, primitive vectors and unit cell. (b) Reciprocal lattice, reciprocal lattice vectors, high symmetry points (Γ, K', M', K), first BZ (white hexagon), and 2 × 2 and 1 × 1 graphene BZs. (c) G-projected band structure, compared to the σ and π band dispersions of (1 × 1) G, along the $\Gamma K' M' K$ path [green arrow in (b)]; the horizontal dashed line marks the vertex of the Dirac cone. (d) and (e) Real-space probability density ρ, projected along the normal coordinate z to the G plane, for an electron at the Γ and K points occupying the band states of different symmetry, indicated by arrows in (c).

(LDA) [26]. The plane-wave basis set (with a cutoff energy of 25 Hartree) was used to expand the valence electron density [27,28], while the core electrons of C and Pt atoms were replaced by Troullier-Martins norm-conserving pseudopotentials [29]. The G/Pt(111) interface was modeled by repeated six-layer thick slabs of Pt(111), terminated on one side by the G overlayer in a commensurate lattice. A slab separation of ∼20 Å was chosen to have both negligible interactions between the replicas and acceptable computational costs. The unit cell of the composite system was built up by optimizing the lattice constants and interlayer distances of a (2 × 2) supercell of graphene (made of eight C atoms) over a ($\sqrt{3} \times \sqrt{3}$) supercell of platinum [containing 18 Pt atoms, 3 per Pt(111) layer]. First, the lattice constant of the Pt supercell was optimized to a value, which turned out to differ by less than 1% from the known Pt-bulk value of 3.92 Å [31]. Secondly, the nearest neighbor distance in the G supercell was set to 1.39 Å in order to generate a commensurate lattice. Third, the out of plane coordinates of the G sheet and of the first Pt layer where optimized, while keeping the other coordinate constant, i.e., the in plane positions of all atoms, as well as the out-of-plane positions of the remaining five Pt layers. As a result, the G and Pt supercells were separated by a distance of 3.30 Å, which is in very good agreement with measurements [11] and other DFT approaches [12,17,32], while the first Pt layer was displaced outwards of ∼7.5% with respect to the inter-layer distance of the other Pt layers in the Pt supercell. On the other hand, freestanding graphene was modeled by repeated slabs generated by the (1 × 1) unit cell with the same C-C distances and slab spacing of the G/Pt(111) calculation. Notice that the C-C nearest-neighboring value used here is ∼2% smaller than the one generally adopted in tight-binding models of graphene (1.42 Å [30]). Ground-state density calculations and geometry optimizations were restricted to Brillouin zone (BZ) integrations on unshifted Monkhorst-Pack grids [33] with ∼800 points×Å^2. In other words, 30 × 30 × 1 and 60 × 60 × 1 grid points were selected for G/Pt(111) and freestanding graphene, respectively, covering the (2 × 2) and (1 × 1) hexagonal BZs shown in Fig. 2(b). The ground-state density for the optimized configuration [Fig. 2(a)] was used to calculate the Kohn-Sham (KS) one electron energies and wave functions along the $\Gamma - K' - M' - K$ path in the BZ [green arrow in Fig. 2(b)].

III. RESULTS AND DISCUSSION

The Pt(997) surface is composed by (111) parallel terraces, containing nine atomic rows, separated by [1$\bar{1}$0] steps [Fig. 1(a)]. The miscut angle, i.e., the angle between [111] and [997] is of 6.45° [34,35]. The low-energy electron diffraction (LEED) image of Pt(997) [Fig. 1(b), top] is composed by

an hexagonal arrangement of spots belonging to the single terrace, replicated along the axis perpendicular to the step direction (i.e., [11$\bar{2}$]) with a periodicity of about 0.314 Å^{-1}, corresponding to a terrace width of 20.01 Å. When the graphene layer is grown, the LEED image shows weak arcs along an outer ring, more visible in off-normal geometry [Fig. 1(b), bottom], while the Pt spots are almost unchanged. Depending on the preparation procedure, a variety of moiré-like superstructures and multiple domains have been found on Pt(111) [10,12,15,16]. Our LEED images show that the bright center of the arcs is rotated by 30° relative to the sharp Pt spots. This structure, which has been already reported on G/Pt(111) [12], corresponds to a (2 × 2) G overlayer on the (111) terraces. Arc shape spots instead of pointlike ones show that graphene is locally ordered but with different rotational domains on the substrate.

To clarify the interaction mechanism, we analyze the DFT computations performed on (2 × 2) G/Pt(111) with the methods outlined in Sec. II. Figure 2(c) shows the band dispersions of the system (orange points of variable size) along the high-symmetry line Γ-K'-M'-K. The point sizes in the plot are proportional to the probability of finding a ground-state electron, with the corresponding wave vector k and binding energy BE, at small (atomic) distances from the G overlayer. The point size scale was fixed by integrating the mod-squares of the KS wave functions, i.e., the one-electron probability densities in real space, for all sampled k points and BEs, over a volume localized at the (2 × 2) unit cell of graphene [Fig. 2(a)]. The height of such a volume is ±1.5 Å along the perpendicular coordinate to the G plane [see Figs. 2(d) and 2(e)]. In this sense, the band-structure of the G/Pt interface is projected to the G overlayer. We note that the use of the (2 × 2) supercell for G/Pt(111) causes a back-folding of the G bands inside the reduced BZ. To improve the discussion, we also have reported in Fig. 2(c) the band structure for freestanding graphene (blue dashed lines). A comparison between the G-projected bands of G/Pt(111) and the π and σ bands of (1 × 1) G reveals that the σ bands are nearly unaffected by the substrate, with only a slight energy shift being visible. This is due to the strong localization of the σ electrons of G/Pt(111) at the G overlayer; indeed, the large size of the σ band points in Fig. 2(c) reflects the high values of the associated probability integrals for electron localization at the graphene region, ranging from 0.9 to 0.95 [Figs. 2(d) and 2(e)]. The π band points, on the other hand,

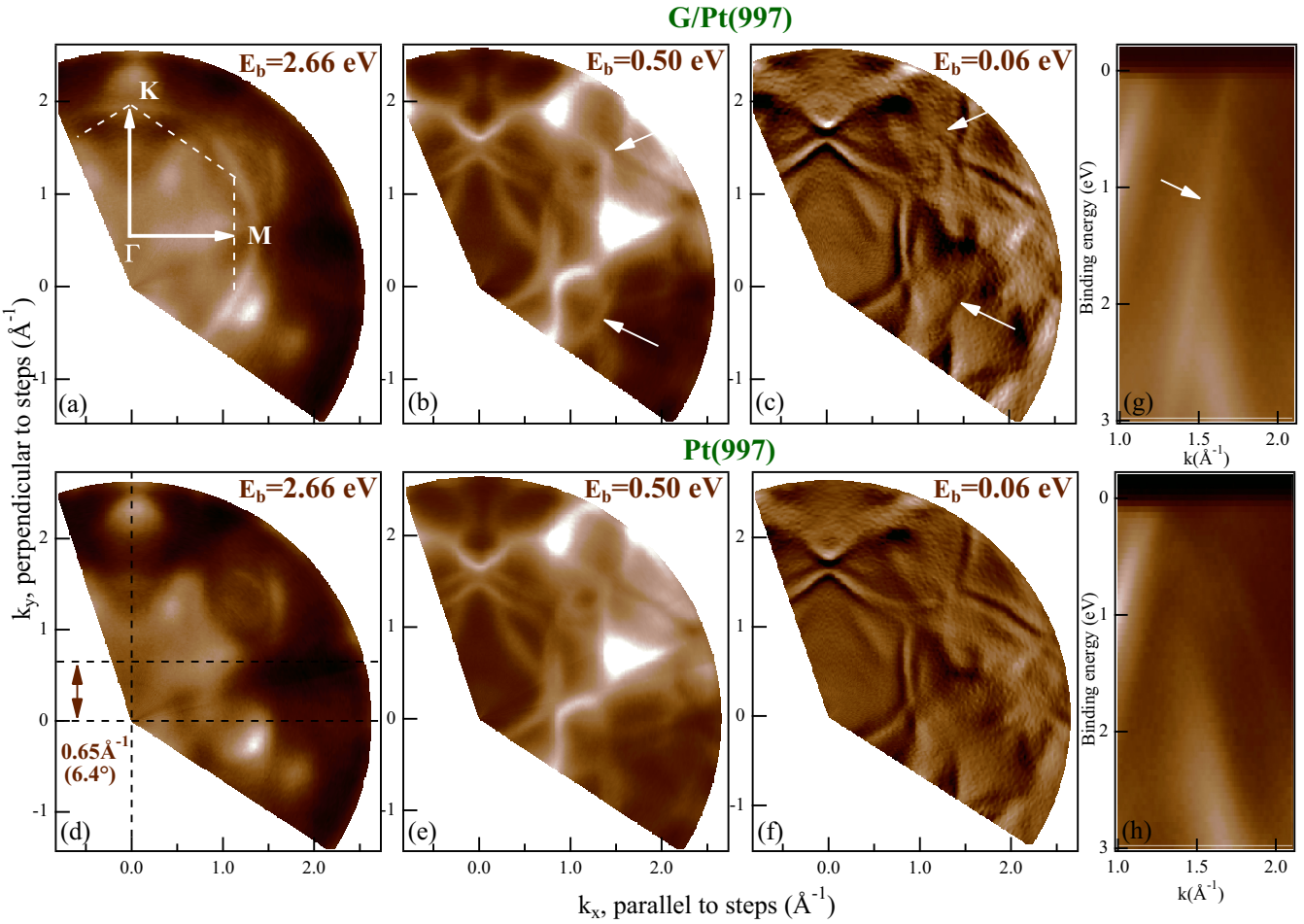

FIG. 3. (Color online) Constant energy images of G/Pt(997) (a)–(c) and Pt(997) (d)–(f), taken at binding energies of 2.66, 0.50, and 0.06 eV, with a photon energy of 126 eV. Images (c) and (f) are shown in first derivative. The y axis is oriented along [11$\bar{2}$]. The high-symmetry directions shown by white arrows in (a) are referred to (2 × 2) G on Pt. ARPES dispersions referred to the microsurface normal of G/Pt(997) (g), and Pt(997) (h), taken at 126 eV of photon energy, along graphene ΓK.

have smaller sizes corresponding to localization probability integrals ranging from 0.5 to 0.6. This indicates that the π electron wave functions have a non-negligible leak into the platinum surface region and can hybridize with the substrate orbitals [Figs. 2(d) and 2(e)]. As a result a more pronounced shift in energy and a slight distortion of the band is observed with respect to the pristine graphene case.

For a better understanding of hybridization effects in G/Pt(111), we consider the real space probability density ρ, projected along the normal coordinate z to the G overlayer, and associated to different band states at the Γ and K points of the BZ [Fig. 2(b)]. In particular, we take the π and σ states of the G overlayer and two specific s and d states of the Pt substrate [denoted s_{Pt} and d_{Pt}, respectively, and indicated by arrows in Fig. 2(c)]. The plots of ρ versus z are reported in Figs. 2(d) and 2(e), where the vertical lines mark the z position of the atomic layers, while the shaded region is the one used to perform the integration for the G-projected band structure appearing in Fig. 2(c). As already pointed out, the one-electron orbitals for the σ bands are sharply peaked at the graphene plane. On the contrary, the π state at the Γ point presents a probability density with non trivial peak structure extending to the first two to three Pt layers below the G plane. The probability of finding a π electron, at Γ, in the Pt region is as large as $\sim$40%. Interestingly, the s_{Pt} state displays a complementary behavior, with a localization probability of $\sim$30% in the G region. By these considerations, we conclude that some hybridization does occur at the Γ point, involving the graphene π band and substrate s bands. As for the π state at the K point, we observe a decreased degree of localization with respect to the σ states. Nevertheless, the associated probability density has the expected symmetry, being centered at the graphene plane and having a negligible intensity inside the substrate. Complementary the d_{Pt} state exhibits a negligible localization at the carbon atoms. Accordingly, the π band preserves its typical, though slightly distorted, linear dispersion at the Fermi level, and the system presents an intact Dirac cone. Last, but not least, it is worth mentioning that our calculation gives a p-doped graphene layer, with the Fermi energy E_F lying at $\sim$0.26 eV below the vertex of the Dirac cone (Fig. 2). Such a result is in fairly good agreement with both previous calculations [17,32], which predicted a p doping of about $\sim$0.3 eV for the same system, and our experimental findings.

Angle-resolved photoemission was employed to characterize the band structure of G/Pt(997). Figure 3 shows constant energy maps of the photoemission signal at selected binding energies of G/Pt(997) (a)–(c) and bare Pt(997) (d)–(f). The main axes were chosen along the steps (k_x), and perpendicularly to them (k_y). By comparing different constant energy images, the graphene π band appears as an arch-shaped contour with intensity peaked at the K points [Fig. 3(a)], and approaching the Fermi level with lower intensity [Fig. 3(c)]. The ARPES dispersion of the π band in proximity of the Fermi level is reported in Fig. 3(g), while Fig. 3(h) shows the corresponding image of pristine Pt(997). According to the LEED image [Fig. 1(b)], the main BZ of graphene is rotated by 30° with respect to that of Pt, indicating a prevalent (2×2) graphene superstructure. This finding is confirmed by the photoemission maps of Fig. 3, showing that the K point of the graphene π band is located along the direction perpendicular to the steps (k_y), where the Pt M point is found. Moreover, the graphene π band, as well as the whole photoemission band patterns observed on constant energy planes, is centered at about 0.65 Å^{-1} along k_y, which indicates a microsurface-centered G electronic structure. This result proves that the graphene layer is locally flat with respect to the single terrace, and thus follows the slope across the step edges. Considering the (111) terraces, different superstructures and rotational domains are present beside the prevalent (2×2). Indeed, in the constant energy image taken in proximity of E_F [Figs. 3(b) and 3(c)], a circular contour is visible (white arrows as guide to the eyes) in agreement with LEED measurements.

Extended valence bands collected along the direction perpendicular to the steps show the band structure of Pt(997) and G/Pt(997) [Fig. 4(a)]. The comparison reveals the presence of the π state of graphene linearly dispersing towards the graphene K point (white dotted line as guide to the eye). The zoom-in of Fig. 4(a) shows that several replicated π bands appear along k_y, displaced by $\Delta k = (0.15 \pm 0.03)$ Å^{-1}. We notice that the width of two Pt terraces is about 40.01 Å, corresponding to $\Delta k = 0.157$ Å^{-1}, very close to the observed periodicity. In Fig. 4(b), we report a top view of several Pt steps and a free-standing graphene layer. Looking at the matching between G and Pt, we observe that the same adsorption geometry replicates with a period corresponding to two Pt terraces. Considering a carpetlike growth over the steps and some unpredictable bending across the step edges, one possible

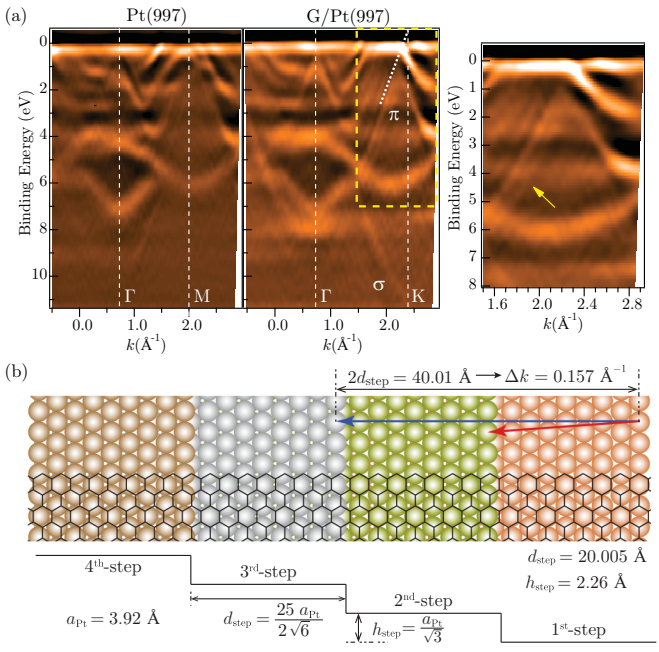

FIG. 4. (Color online) (a) ARPES dispersions of Pt(997) and G/Pt(997), referred to the macrosurface normal, shown in second derivative and taken at 160 eV of photon energy along the direction perpendicular to the steps ($[11\bar{2}]$). The inset on the right-hand side emphasizes the repeated graphene π bands in proximity of the K point. (b) Top-view schematic of graphene adsorbed on Pt(997) showing the absence of periodicity of graphene on one single Pt terrace.

explanation of our ARPES results is that, in order to match equivalent Pt adsorption sites, the graphene layer forms a wavelike pattern with double real-space periodicity.

As pointed out, the π band is microsurface-centered, with a minimum of about 8.3 eV at the microsurface Γ point [Fig. 4(a)]. Going from *strongly* interacting metals, such as Ru(0001) and Ni(111), to *weakly* interacting *5d* ones, e.g., Ir(111) and Pt, the π band minimum is upshifted of about 2 eV, from about 10 eV [3,36] to 8.3 eV in the present measurements. In free-standing graphene the same minimum is expected at 7.69 eV [Fig. 2(c)]. Such a nonrigid shift of the π band with respect to free-standing graphene confirms the theoretical description given in Fig. 2, namely, a partial mixing of the π band with the substrate orbitals. Even though Pt is considered in the literature as belonging to the weakly interacting metals, the hybridization of its substrate orbitals with the π band of graphene must be taken into account. Indeed, recent Raman experiments have shown that, due to a considerable hybridization with the substrate, the Raman signal of G on Pt reveals stronger modifications compared to that of suspended graphene or graphene supported by noble metals [37]. However, in the vicinity of the K point, a linear dispersion is observed [Fig. 4(a)], in agreement with our theoretical description. From a linear best fit to the single branch (not shown), we find that the Dirac point is located at about 0.5 eV above the Fermi level, in agreement with the DFT predictions presented here [Fig. 2(c)] and in refs [17,32]; while from the constant gradient dE/dk of about 7.6 eVÅ, we obtain a group velocity of $\sim 10^6$ m/s, as expected for free-standing graphene. Similar results were obtained from ARPES measurements performed on G/Pt(111) [11]. We finally point out that the absence of band gap and parabolic dispersion of the π band, observed, for example, in Au(778) [23], suggests that nanoribbons are not present in our system.

IV. CONCLUSION

In conclusion, we have shown that graphene can be grown on the vicinal Pt(997) surface by chemical vapor decomposition of ethylene. The graphene layer lies on the surface forming prevalent (2×2) rotated domains with respect to the single (111) terrace. DFT calculations describe a graphene π band strongly localized at the graphene plane close to the Fermi level, while propagating through the bulk at higher binding energies. ARPES measurements show a linearly dispersing π band centered at the microsurface normal, with electron group velocity close to that in freestanding graphene but slightly affected by the Pt bands. Finally, the π band of graphene exhibits repeated band dispersion with $\Delta k = (0.15 \pm 0.03)$ Å^{-1}, suggesting a wavelike growth extending across the step edges with double real-space periodicity compared to the Pt terrace width.

ACKNOWLEDGMENTS

Useful discussion with Valerio Bellini and Fabiano Corsetti are kindly acknowledged. This work has been supported by MIUR (FIRB-Futuro in Ricerca 2010- Project PLASMOGRAPH Grant No. RBFR10M5BT, and PRIN grant 20105ZZTSE), and by the European Science Foundation (ESF) under the EUROCORES Program EuroGRAPHENE. M. Pisarra acknowledges financial support by the European Commission, European Social Fund, and Regione Calabria, (POR) Calabria - FSE 2007/2013.

[1] S. M. Kozlov, F. Viñes, and A. Görling, J. Phys. Chem. C **116**, 7360 (2012).
[2] E. Voloshina and Yu. Dedkov, Phys. Chem. Chem. Phys. **14**, 13502 (2012).
[3] D. Pacilé, P. Leicht, M. Papagno, P. M. Sheverdyaeva, P. Moras, C. Carbone, K. Krausert, L. Zielke, M. Fonin, Y. S. Dedkov, F. Mittendorfer, J. Doppler, A. Garhofer, and J. Redinger, Phys. Rev. B **87**, 035420 (2013).
[4] Yu. S. Dedkov and M. Fonin, New J. Phys. **12**, 125004 (2010).
[5] A. Varykhalov, D. Marchenko, J. Sánchez-Barriga, M. R. Scholz, B. Verberck, B. Trauzettel, T. O. Wehling, C. Carbone, and O. Rader, Phys. Rev. X **2**, 041017 (2012).
[6] M. Papagno, S. Rusponi, P. M. Sheverdyaeva, S. Vlaic, M. Etzkorn, D. Pacilé, P. Moras, C. Carbone, and H. Brune, ACS Nano **6**, 199 (2012).
[7] E. Starodub, A. Bostwick, L. Moreschini, S. Nie, F. El Gabaly, K. F. McCarty, and E. Rotenberg, Phys. Rev. B **83**, 125428 (2011).
[8] M. Kralj, I. Pletikosić, M. Petrović, P. Pervan, M. Milun, A. T. N'Diaye, C. Busse, T. Michely, J. Fujii, and I. Vobornik, Phys. Rev. B **84**, 075427 (2011).
[9] S. Ulstrup, L. Nilsson, J. A. Miwa, R. Balog, M. Bianchi, L. Hornekaer, and P. Hofmann, Phys. Rev. B **88**, 125425 (2013).
[10] A. B. Preobrajenski, M. L. Ng, A. S. Vinogradov, and N. Mårtensson, Phys. Rev. B **78**, 073401 (2008).
[11] P. Sutter, J. T. Sadowski, and E. Sutter, Phys. Rev. B **80**, 245411 (2009).
[12] M. Gao, Y. Pan, L. Huang, H. Hu, L. Z. Zhang, H. M. Guo, S. X. Du, and H.-J. Gao, Appl. Phys. Lett. **98**, 033101 (2011).
[13] S. Rajasekaran, S. Kaya, T. Anniyev, H. Ogasawara, and A. Nilsson, Phys. Rev. B **85**, 045419 (2012).
[14] A. Politano, A. R. Marino, V. Formoso, D. Farías, R. Miranda, and G. Chiarello, Phys. Rev. B **84**, 033401 (2011).
[15] Z. Hu, D. Ogletree, M. V. Hove, and G. Somorjai, Surf. Sci. **180**, 433 (1987).
[16] H. Ueta, M. Saida, C. Nakai, Y. Yamada, M. Sasaki, and S. Yamamoto, Surf. Sci. **560**, 183 (2004).
[17] P. A. Khomyakov, G. Giovannetti, P. C. Rusu, G. Brocks, J. van den Brink, and P. J. Kelly, Phys. Rev. B **79**, 195425 (2009).
[18] X. Y. Wang, X. J. Shen, and R. M. Osgood, Jr., Phys. Rev. B **56**, 7665 (1997).
[19] A. M. Shikin, A. Varykhalov, G. V. Prudnikova, V. K. Adamchuk, W. Gudat, and O. Rader, Phys. Rev. Lett. **93**, 146802 (2004).
[20] A. Mugarza, A. Mascaraque, V. Pérez-Dieste, V. Repain, S. Rousset, F. J. Garcia de Abajo, and J. E. Ortega, Phys. Rev. Lett. **87**, 107601 (2001).
[21] J. E. Ortega, S. Speller, A. R. Bachmann, A. Mascaraque, E. G. Michel, A. Närmann, A. Mugarza, A. Rubio, and F. J. Himpsel, Phys. Rev. Lett. **84**, 6110 (2000).

[22] Y.-W. Son, M. Cohen, and S. Louie, Phys. Rev. Lett. **97**, 216803 (2006).
[23] P. Ruffieux, J. Cai, N. C. Plumb, L. Patthey, D. Prezzi, A. Ferretti, E. Molinari, X. Feng, K. Müllen, C. A. Pignedoli, and R. Fasel, ACS Nano **6**, 6930 (2012).
[24] S. Linden, D. Zhong, A. Timmer, N. Aghdassi, J. H. Franke, H. Zhang, X. Feng, K. Müllen, H. Fuchs, L. Chi, and H. Zacharias, Phys. Rev. Lett. **108**, 216801 (2012).
[25] A. M. Shikin, S. A. Gorovikov, V. K. Adamchuk, W. Gudat, and O. Rader, Phys. Rev. Lett. **90**, 256803 (2003).
[26] J. P. Perdew and A. Zunger, Phys. Rev. B **23**, 5048 (1981).
[27] X. Gonze *et al.*, Comp. Mater. Scie. **25**, 478 (2002).
[28] X. Gonze *et al.*, Z. Kristallogr. **220**, 558 (2005).
[29] N. Troullier and J. L. Martins, Phys. Rev. B **43**, 1993 (1991).
[30] R. Saito, G. Dresselhaus, and M. S. Dresselhaus, *Physical Properties of Carbon Nanotubes* (Imperial College Press, London, 1998).
[31] N. W. Ashcroft and N. D. Mermin, *Solid State Physics* (Hault Saunders, Philadelphia, 1976).
[32] G. Giovannetti, P. A. Khomyacov, G. Brooks, V. M. Karpan, J. van den Brink, and P. J. Kelly, Phys. Rev. Lett. **101**, 026803 (2008).
[33] H. J. Monkhorst and J. D. Pack, Phys. Rev. B **13**, 5188 (1976).
[34] A. Dallmeyer, C. Carbone, W. Eberhardt, C. Pampuch, O. Rader, W. Gudat, P. Gambardella, and K. Kern, Phys. Rev. B **61**, R5133 (2000).
[35] G. Prévot, L. Barbier, and P. Steadman, Surf. Sci. **604**, 1265 (2010).
[36] M. Papagno, D. Pacilé, P. D. Topwal, P. Moras, P. M. Sheverdyaeva, F. D. Natterer, A. Lehnert, S. Rusponi, Q. Dubout, F. Calleja, E. Frantzeskakis, S. Pons, J. Fujii, I. Vobornik, M. Grioni, C. Carbone, and H. Brune, ACS Nano **6**, 9299 (2012).
[37] Q. Zhou, S. Coh, M. L. Cohen, S. G. Louie, and A. Zettl, Phys. Rev. B **88**, 235431 (2013).